Virologica Sinica 40 (2025) 247–259

Contents lists available at ScienceDirect

Virologica Sinica

journal homepage: www.keaipublishing.com/en/journals/virologica-sinica
www.virosin.org

Research Article

Artemisia annua L. leaf extracts suppress influenza virus infection by targeting the viral nucleoprotein and blocking mitochondria-mediated apoptosis

Xiwen Zhao [a,b], Xuan Dai [b], Fuyi Wang [b,c], Chenyang Li [c], Xun Song [d], Yingying Han [c], Chaowei Zhang [c], Lu Wang [e,*], Zhendan He [d,*], Rongping Zhang [a,*], Liang Ye [b,*]

[a] College of Chinese Medicine, School of Chinese Materia Medica and Yunnan Key Laboratory of Southern Medicine Utilization, Yunnan University of Chinese Medicine, Kunming 650500, China
[b] Department of Immunology, International Cancer Center, Shenzhen University Medical School, Shenzhen 518055, China
[c] College of Pharmacy, Shenzhen University Medical School, Shenzhen 518055, China
[d] College of Pharmacy, Shenzhen Technology University, Shenzhen 518118, China
[e] Hyperbaric Oxygen Department, Shenzhen University General Hospital, Shenzhen 518055, China

ARTICLE INFO

Keywords:
Artemisia annua L
Influenza A virus (IAV)
Nucleoprotein (NP)
Mitochondrial apoptosis

ABSTRACT

Artemisia annua L. is a medicinal herb with multiple therapeutic applications, whereas its anti-influenza A virus (IAV) efficiency and mechanism of action are still unclear. Here, we investigated the inhibition activity and mechanism of *A. annua* leaf methanol extracts (AALME) against IAV *in vitro* and *in vivo*. Our results revealed that AALME exhibits potent anti-IAV activity by interacting with IAV particles. Mechanistically, AALME directly targets the IAV nucleoprotein (NP) protein and abolishes the nuclear import of IAV NP. AALME profoundly suppresses IAV-induced mitochondrial apoptosis via suppressing ROS-mediated AIF-dependent pathways. More importantly, we found that AALME plays a crucial role in protecting mice from IAV infection and mitigating IAV pathogenicity. This current work provides mechanistic insight into the mechanism by which AALME controls IAV infection *in vitro* and *in vivo*, potentially contributing to the development of antiviral treatments for IAV infection.

INTRODUCTION

Influenza A virus (IAV) is a major respiratory pathogen that has caused devastating global pandemics in humans and other animal species, while seasonal flu epidemics are responsible for approximately 500,000 deaths each year (Medina and García-Sastre, 2011). The genome of IAV is composed of eight single-stranded negative-sense RNA segments that encode RNA polymerase subunits (PB1, PB2, and PA), viral surface glycoproteins hemagglutinin (HA) and neuraminidase (NA), matrix protein (M1), membrane protein (M2), viral nucleoprotein (NP), the nonstructural protein NS1, and nuclear export protein (NEP) (Krammer et al., 2018). IAVs are usually classified by HA and NA, which mediate receptor binding and virus release. The M2 protein is a proton ion channel that is required for the assembly of IAV and the uncoating of the viral core during entry. NP is involved in various stages of the viral life cycle, including ribonucleoprotein (RNP) formation, viral transcription, replication, and virion assembly. Targeting NP may be an appealing strategy for antiviral treatment (Krammer et al., 2018). Indeed, only three classes of anti-IAV drugs are now approved for the treatment of influenza, including M2 ion channel inhibitors (amantadine and rimantadine), NA inhibitors (oseltamivir, peramivir, and zanamivir), and PA inhibitors (baloxavir marboxil). However, increasing amounts of mutant viruses with resistance to these inhibitors have been identified (Guan and Chen, 2005; Imai et al., 2020), implying that novel anti-IAV drugs are urgently needed.

Medicinal plants are being shown to have more profound and beneficial effects than previously assumed in recent years. Among them, *Artemisia annua* L., as an Asteraceae family member, has been widely employed in traditional Chinese medicine to treat a range of diseases. *A. annua* extract provides protection against *Toxoplasma gondii*

* Corresponding authors.
E-mail addresses: liangyeszu@163.com (L. Ye), zhrpkm@163.com (R. Zhang), hezhendan@126.com (Z. He), luwangszu@163.com (L. Wang).

https://doi.org/10.1016/j.virs.2025.03.001
Received 27 September 2024; Accepted 26 February 2025
Available online 3 March 2025

(de Oliveira et al., 2009), *Leishmania* (Islamuddin et al., 2015), *Acanthamoeba* (Wojtkowiak-Giera et al., 2019), and *Schistosoma* (Ferreira et al., 2011). Apart from its capacity to tackle parasite infections, *A. annua* possesses antibacterial (Juteau et al., 2002; Marinas et al., 2015), antitumor (Chen et al., 2014; Kim et al., 2017), and antiviral (Karamoddini et al., 2011; Nie et al., 2021) properties. It was also shown that ethanolic extracts of *A. annua* from various locations throughout the world exhibited antiviral activity against SARS-CoV-1, SARS-CoV-2, and their variants *in vitro*, although the potential mechanism of action is largely unclear (Nie et al., 2021).

A. annua contains various flavonoids, terpenoids, coumarins, caffeoylquinic acids, acetylenes, and sterols (Shojaii and Ghods, 2021). Artemisinin, one of the most well-known flavonoids from *A. annua*, has been utilized for treating malaria, but its anti-IAV activity *in vitro* is weak or has no inhibitory role (Efferth, 2018). However, some semi-synthetic artemisinin derivatives have been reported to show anti-IAV activities. Artesunate, a semisynthetic derivative of artemisinin derived from *A. annua*, can induce cAMP accumulation via inhibiting PDE4, reduce ERK phosphorylation, and consequently block IAV vRNP export, eventually suppressing IAV replication (Yang et al., 2023). Dihydroartemisenin, which is also one of the artemisinin derivatives, inhibits IAV-induced TNF-α and IL-6 expression in BEAS-2B cells through the ERK signaling pathway (Ou et al., 2020). However, to date, there are no reports on the anti-IAV effects of natural *A. annua* extract. Therefore, in this study, we aimed to investigate the procedure and its integration of the anti-IAV effect of *A. annua* extract in different host cells and explore the antiviral mechanism *in vitro* and *in vivo*.

RESULTS

The characteristic components of *A. annua* leaf

To identify the chemical components of *Artemisia annua* L. leaf, we prepared *A. annua*. leaf methanol extracts (AALME) for ultrahigh-performance liquid chromatography tandem mass spectrometry (UPLC-MS/MS). The chemical base peak ion (BPI) chromatogram of AALME was divided into two categories based on the positive and negative ion modes of UPLC-MS/MS, as illustrated in Fig. 1A. In comparison to a standard database (Orbitrap, TCM), we identified 149 chemical compounds, including 41 flavonoids, 24 terpenoids, 27 organic compounds, 23 phenylpropanoids, 17 alkaloids, 11 phenolic acids, 5 phenols, and 10 quinones (Fig. 1B). The detailed information on the 149 compounds is further summarized in Supplementary Table S2. Notably, the majority of those compounds have been reported to have immunomodulatory and antiviral activities (Özçelik et al., 2011; Badshah et al., 2021; Song et al., 2021; Abookleesh et al., 2022), implying that AALME may have anti-IAV effects.

Cytotoxicity of AALME

The cytotoxicity of AALME was investigated in various IAV-sensitive host epithelial cells, such as MDCK and A549 cells. The CC_{50} values of AALME against MDCK and A549 cells were 202.9 and 258.6 μg/mL, respectively (Fig. 2). Meanwhile, baloxavir marboxil was used as a positive control drug, and its cytotoxicity was evaluated. The CC_{50} values of baloxavir marboxil against MDCK and A549 cells were 3.9 and

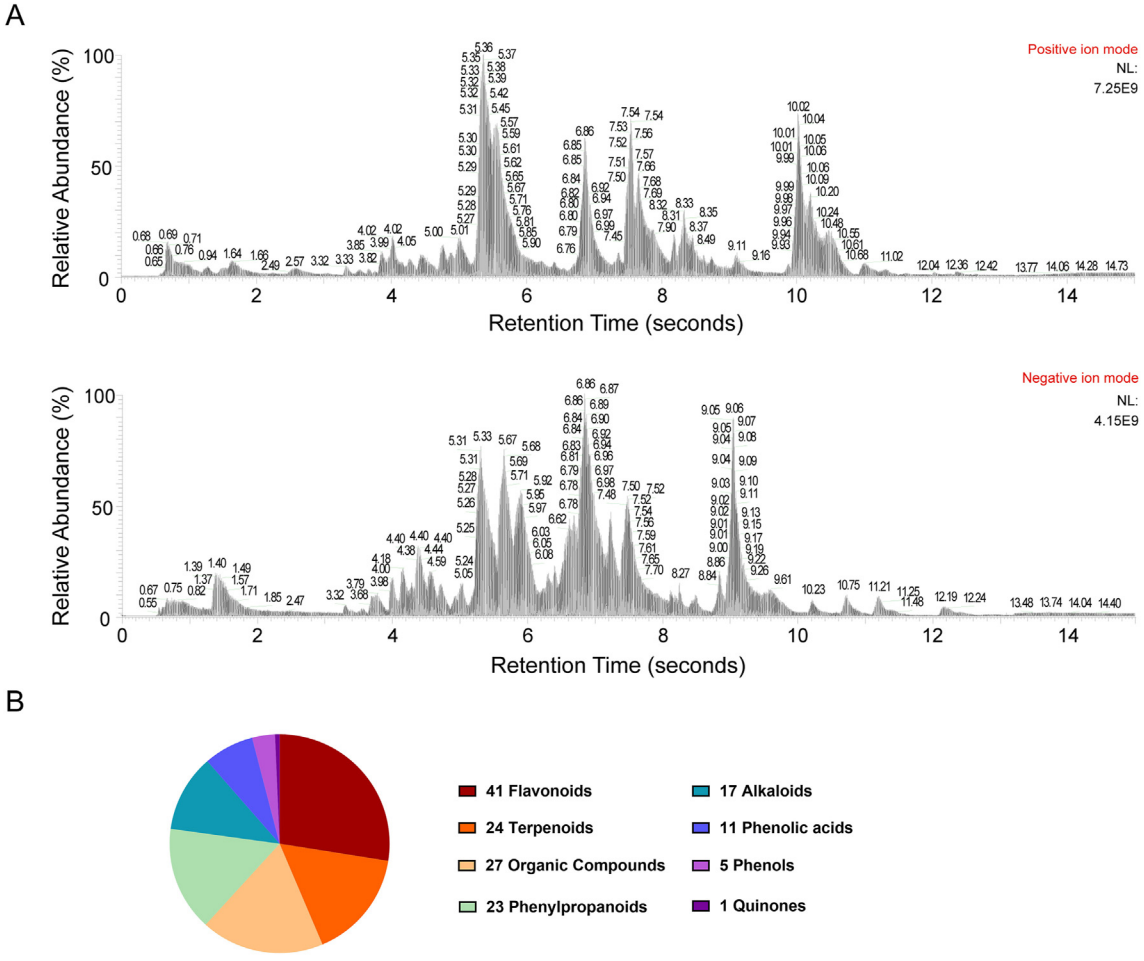

Fig. 1. Ultrahigh-performance liquid chromatography-tandem mass spectrometry (UPLC-MS/MS) for the identification of AALME chemical compounds. **A** The chemical base peak ion (BPI) chromatogram of AALME in the positive and negative ion modes. **B** Structural classification of compounds in AALME.

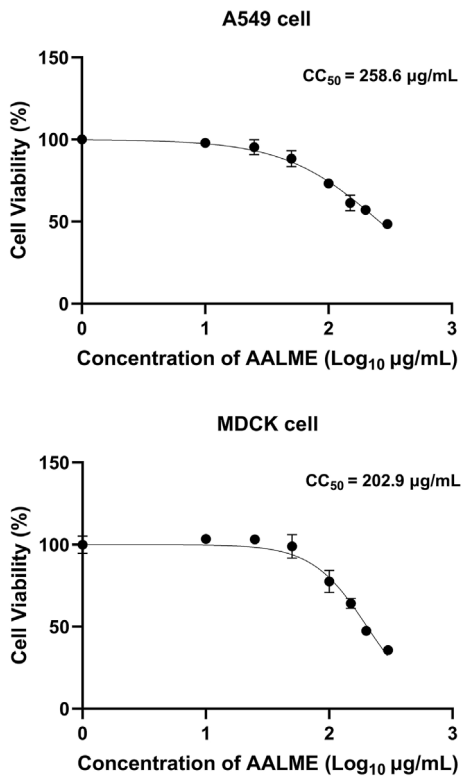

Fig. 2. Effect of AALME on cell viability of IAV host cells. Influenza virus-sensitive MDCK and A549 cells were treated for 24 h with various concentrations of AALME (0, 10, 25, 50, 100, 150, 200, and 300 μg/mL), and the 50% cytotoxic concentration (CC_{50}) value of AALME cell viability was determined by the CCK-8 assay. Data are presented as mean ± SD (n = 6).

4.8 μg/mL, respectively (Supplementary Fig. S1). We further evaluated the safe concentration of AALME and baloxavir marboxil using a cell cytopathic effects (CPE) assay, which showed no cytopathic effects at doses of 25 μg/mL and 0.4 μg/mL, respectively (Supplementary Fig. S2). As a result, the maximal doses of AALME (25 μg/mL) and baloxavir marboxil (0.4 μg/mL) were used in the subsequent experiments.

AALME inhibits IAV replication *in vitro*

To determine the antiviral activity of AALME, we initially investigated the effects of AALME on influenza virus (IAV)-induced CPE in MDCK and A549 cells. The results demonstrated that AALME effectively inhibited IAV-induced CPE formation in MDCK and A549 cells in a dose-dependent manner (Fig. 3A and B), which is consistent with the findings that AALME treatment of the IAV-infected MDCK cells resulted in a dose-dependent reduction in viral titers (Fig. 3C). Importantly, the antiviral efficacy of 25 μg/mL of AALME was comparable to that of 0.4 μg/mL of baloxavir marboxil (Fig. 3A and C). These results indicated that AALME could potently suppress IAV replication. In addition, we assessed the inhibition capability of AALME against the IAV in MDCK and A549 cells by Western blot and RT-qPCR. We found that AALME dose-dependently diminished viral *M2*, *HA*, and *NP* mRNA expression in MDCK and A549 cells (Fig. 3D and E). Concomitantly, these results were further confirmed by the reduction of viral HA and NP synthesis in IAV-infected MDCK and A549 cells upon AALME treatment in a dose-dependent manner (Fig. 3F and G). Thus, AALME demonstrated potent activity against IAV *in vitro*.

AALME possesses direct anti-IAV properties

Next, we devised three different modes to evaluate the inhibitory effects of AALME on the IAV life cycle, which are premixed, prophylactic, and therapeutic administrations. Our results showed that premixing AALME with IAV markedly reduced the IAV-induced CPE development and viral HA and NP protein levels in MDCK cells (Fig. 4A). However, AALME fails to dampen IAV-induced CPE generation and viral HA and NP protein synthesis during prophylactic and therapeutic administrations (Fig. 4B and C). Given that premixed administration of AALME effectively reduced viral replication in host cells, we aimed to further investigate how AALME affects the life cycle of H1N1 influenza virus. We administered AALME separately during the virus adsorption and internalization phases and detected the expression levels of *HA*, *NP*, and *M2* mRNA in MDCK cells 10 h after infection. We found that AALME significantly inhibited the expression of *HA*, *NP*, and *M2* genes, suggesting AALME inhibited the IAV during both the adsorption and internalization stages (Supplementary Fig. S3). In line with these findings, AALME did not improve the mRNA expression of major innate antiviral host factors such as type I interferons (*IFN-α1* and *IFN-β1*), type III interferons (*IFN-λ1* and *IFN-λ2/3*), as well as interferon-stimulated genes (*Mx1* and *Oas2*) *in vitro* and *in vivo* (Supplementary Fig. S4). Therefore, these results suggest that AALME confers anti-IAV effects by directly interacting with IAV particles.

AALME targets IAV NP and prevents IAV NP nuclear imports

Since AALME may directly interact with IAV virions, we further explored the underlying mechanism by detecting kinetic binding sensorgrams of increasing concentrations of AALME from 50 to 100 μg/mL to IAV-related proteins (HA, NA, NS1, and NP) using biolayer interferometry (BLI). The association/dissociation curves suggested that AALME markedly binds with IAV NP rather than other proteins (HA, NA, or NS1) (Fig. 5A). To verify the affinity of AALME and NP, we employed the cellular thermal shift assay (CETSA). The results demonstrated an increase in the thermal stability of the NP protein after AALME treatment (Fig. 5B), confirming a strong binding affinity between AALME and IAV NP. It is generally recognized that NP, as a major component of the vRNP complex of the H1N1 influenza virus, plays an important role in vRNP nuclear trafficking. We assessed the localization of NP in MDCK cells at 1, 2, and 4 h after IAV infection by confocal immunofluorescence microscopy and revealed that AALME blocked the nuclear accumulation of NP in MDCK cells and retained NP to the cytoplasm 2–4 h after IAV infection (Fig. 5C–E). As further support, the Western blot data confirmed that AALME inhibited nuclear NP protein levels in IAV-infected MDCK cells (Fig. 5F and G). Overall, these findings suggest that AALME could interact with IAV NP and abolish the nuclear import of NP.

AALME prevents IAV-induced mitochondrial apoptosis by regulating the ROS-AIF axis

Numerous studies have proven that viral infection can result in apoptosis (Clarke and Tyler, 2009; Atkin-Smith et al., 2018). We employed Annexin V and PI staining, which are conventional approaches for determining early and late-phase apoptosis, to see if IAV infection caused cell apoptosis that might be reversed by AALME. The result showed that AALME clearly inhibits IAV-induced early and late apoptotic processes in A549 cells (Fig. 6A and B). We next assessed whether the inhibitory role of AALME in IAV-induced apoptosis is attributed to mitochondrial pathway-mediated apoptosis. A549 cells were infected with IAV in the presence or absence of AALME, and the changes in mitochondrial membrane potential (MMP) were measured using the fluorescent MMP probe JC-1 by flow cytometry. The results revealed that AALME is capable of inhibiting the decrease of MMP caused by IAV in A549 cells (Fig. 6C). Reactive oxygen species (ROS) are generated in mitochondria by virus-infected cells, which are responsible for apoptosis. We therefore investigated whether the anti-mitochondrial apoptotic effect of AALME depends on ROS generation. To assess the intracellular ROS levels in IAV-infected A549 cells treated with or without AALME, we found that the cellular ROS content significantly decreased in

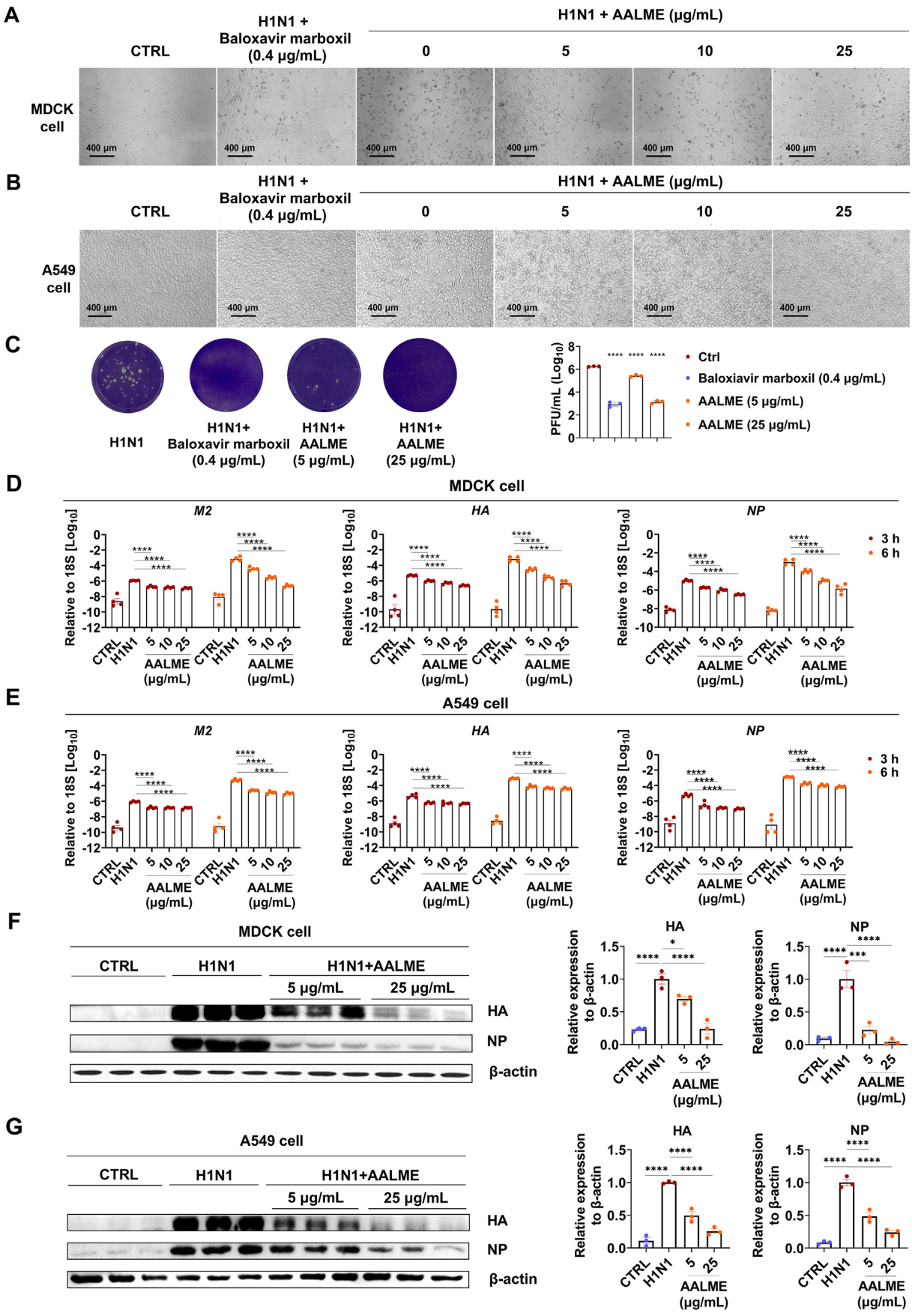

(caption on next page)

Fig. 3. AALME exhibits potent anti-IAV activity *in vitro*. **A, B** H1N1 virus PR8 (MOI = 0.05) was incubated with AALME (0, 5, 10, and 25 μg/mL) or baloxavir marboxil (0.4 μg/mL) at 4 °C for 2 h. MDCK and A549 cells were cultured with the mixture for 2 h at 37 °C, followed by a 24-h incubation with AALME (0, 5, 10, and 25 μg/mL) or baloxavir marboxil (0.4 μg/mL). A virus-induced cytopathic effect (CPE) was observed by a microscope. Scale bars, 400 μm. **C** H1N1 virus PR8 (MOI = 0.05) was incubated with AALME (5 and 25 μg/mL) or baloxavir marboxil (0.4 μg/mL) for 2 h at 4 °C and then cultured with MDCK cells for 2 h at 37 °C. The inoculum was replenished by AALME or baloxavir marboxil incubation for 12 h at 37 °C and subjected to a viral plaque assay. Data are expressed as the mean ± SEM (n = 3). **D, E** H1N1 virus PR8 (MOI = 0.05) and AALME were mixed for 2 h at 4 °C before being added to MDCK and A549 cells for 2 h at 37 °C. The inoculum was replenished with AALME and incubated at 37 °C for 3 or 6 h. The mRNA expression levels of viral genes *M2, HA,* and *NP* were determined by RT-qPCR. Data are shown as the mean ± SEM (n = 4). **F, G** H1N1 virus PR8 (MOI = 0.05) and AALME were mixed and incubated at 4 °C for 2 h before being added to MDCK and A549 cells and incubated at 37 °C for 2 h. The inoculum was removed and replaced by AALME, which was incubated at 37 °C for 12 h. The levels of viral HA and NP proteins were analyzed by western blotting. Results are represented as the ratio of the specific protein to the β-actin protein (n = 3). ns, no significant difference; *$P < 0.05$, ***$P < 0.001$, ****$P < 0.0001$ by one-way ANOVA with Dunnett's multiple comparisons test.

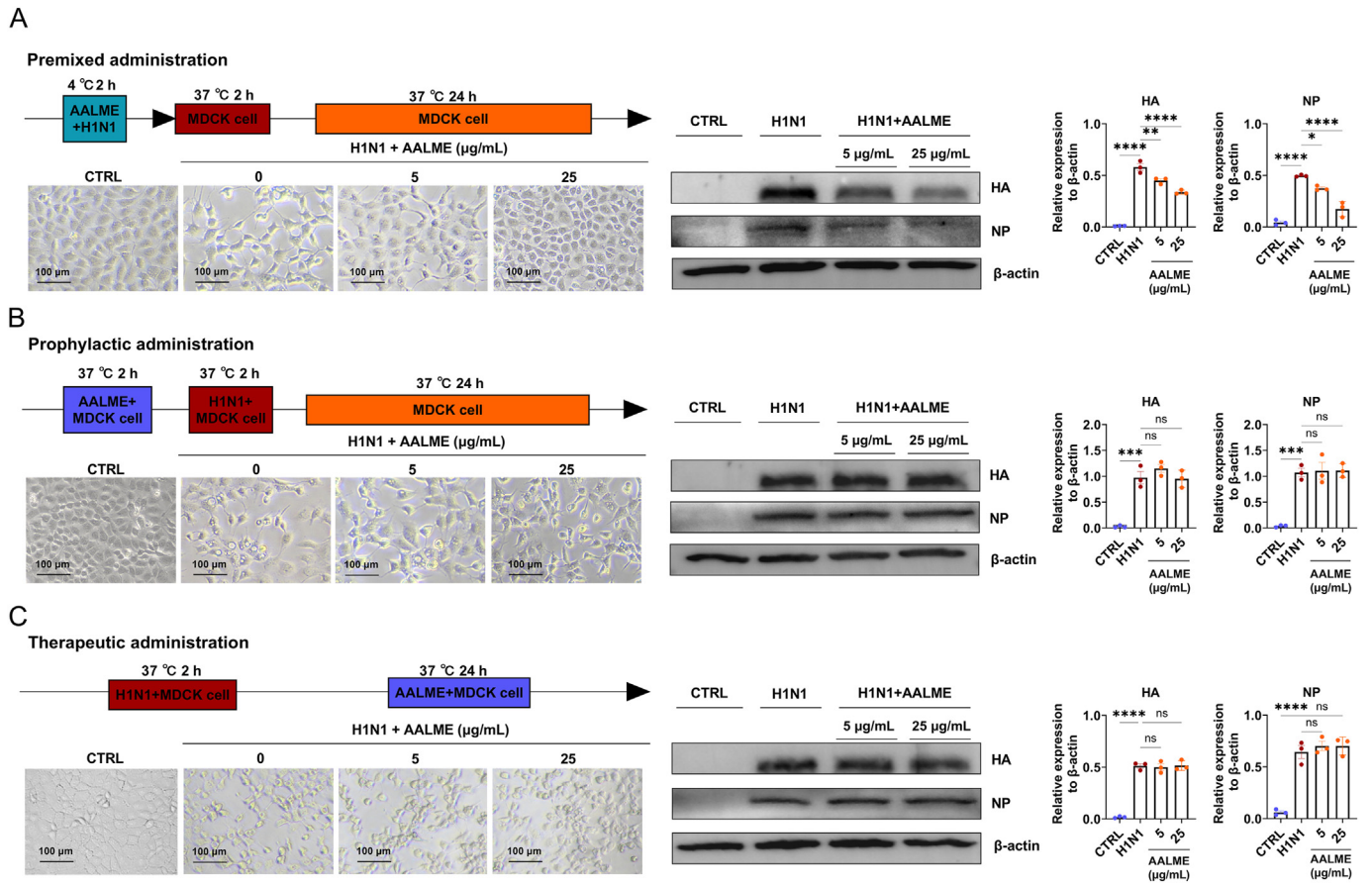

Fig. 4. Effects of different AALME treatment conditions on IAV infection. **A** Premixed administration. H1N1 virus PR8 (MOI = 0.05) and AALME (0, 5, and 25 μg/mL) were mixed and incubated for 2 h at 4 °C. MDCK cells were incubated with the mixture at 37 °C for 2 h, then the mixture was removed and replaced with fresh medium. The cells were then incubated at 37 °C for 24 h. **B** Prophylactic administration. MDCK cells were incubated with AALME (0, 5, and 25 μg/mL) for 2 h at 37 °C before being infected with the H1N1 virus PR8 (MOI = 0.05). The inoculum was then replaced with fresh medium, and the cells were incubated at 37 °C for 24 h. **C** Therapeutic administration. MDCK cells were initially challenged with H1N1 virus PR8 (MOI = 0.05), then incubated with AALME (0, 5, and 25 μg/mL) for 24 h at 37 °C after the viral supernatant was removed. Following the foregoing procedures, CPE was viewed under a microscope. Scale bars, 100 μm. The expression levels of HA and NP proteins were determined by western blotting. Results are shown as the ratio of the specific protein to the β-actin protein and the mean ± SEM of triplicate samples. ns, no significant difference. *$P < 0.05$, **$P < 0.01$, ***$P < 0.001$, ****$P < 0.0001$ by one-way ANOVA with Dunnett's multiple comparisons test.

AALME-treated A549 cells. More importantly, AALME restrains IAV-triggered ROS production in A549 cells (Fig. 6D). To rule out the possibility that the observed reduction in ROS production could be attributed to the decreased viral load, we utilized Rosup to stimulate ROS production. The results showed that AALME greatly reduced ROS generation caused by Rosup, indicating that the inhibitory role of AALME in IAV-induced ROS production was independent of its ability to block viral replication (Fig. 6E).

To confirm the notion that the mitochondrial apoptotic pathway is essential for AALME-cutting IAV-mediated apoptosis, we explored the levels of apoptosis-related proteins. As expected, AALME dramatically decreases the expression of IAV-induced pro-apoptotic proteins Bad and Bax while elevating the expression of the anti-apoptotic protein Bcl-xl (Fig. 6F). Interestingly, AALME can strongly restrain the expression of IAV-induced apoptosis-inducing factor (AIF) (Fig. 6F), which is involved in initiating the caspase-independent pathway of apoptosis. These findings demonstrate that AALME-restrained mitochondrial apoptosis in response to IAV infection via suppressing the ROS-mediated AIF-dependent pathway.

AALME exhibits anti-IAV properties *in vivo*

To investigate the role of AALME in IAV infection *in vivo*, mice were intranasally infected with or without A/PR8/8/34 influenza virus, either mixed or unmixed with AALME (1 and 10 mg/kg), and administered

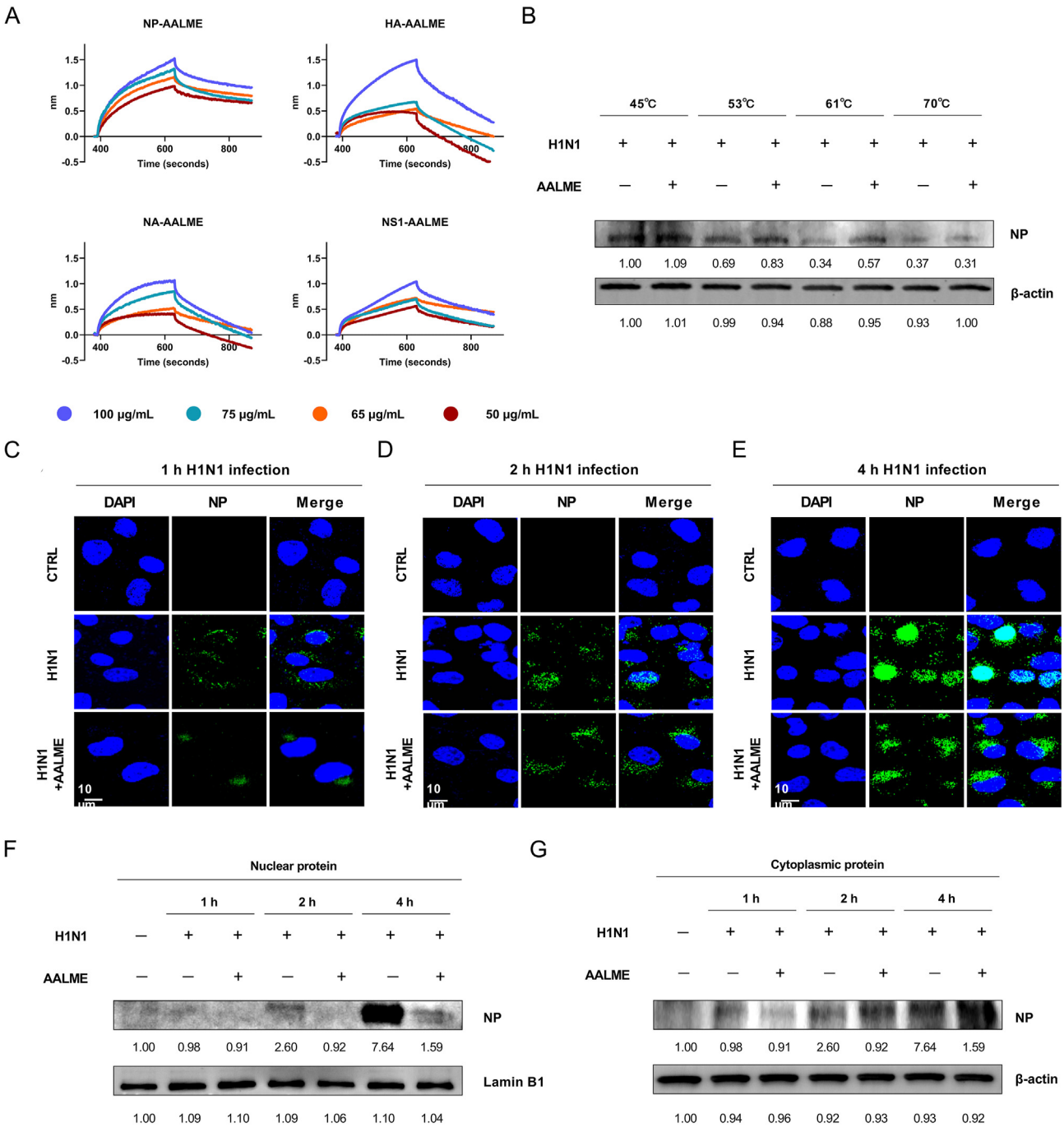

Fig. 5. AALME interacts with IAV NP and limits its nuclear localization. **A** Biolayer Interferometry (BLI) was used to assess the binding kinetics of AALME with the immobilized IAV NP, HA, NA, and NS1. The loading step of AALME was carried out for 240 s, which was followed by 240 s of baseline stabilization. **B** Cellular thermal shift assay (CETSA) for determining the AALME binding affinity with IAV NP. **C–E** H1N1 virus PR8 (MOI = 0.05) was combined with AALME (25 μg/mL) and incubated for 2 h at 4 °C before being given to MDCK cells for 1, 2, or 4 h at 37 °C. Cells were fixed, and DAPI staining and mouse anti-IAV NP antibodies were utilized to define the locations of the nucleus and viral NP, respectively. The merged image was enlarged further and displayed on the right. **F, G** Nuclear and cytoplasmic proteins from different time points post-infection are extracted, and IAV NP quantification was evaluated by western blotting. Lamin B1 was the internal reference for nuclear proteins, while β-actin was the internal reference for cytoplasmic proteins.

AALME (1 and 10 mg/kg) intranasally for three days, while the control group received oseltamivir (1 and 10 mg/kg) or PBS. Changes in body weight and survival rates of the mice were monitored over a period of 15 days after infection. The results demonstrated that ALLME dramatically reduced IAV-induced weight loss in mice and increased the survival rate of IAV-infected mice, which was consistent with the antiviral effect of oseltamivir (Fig. 7A and B). On day three following the IAV infection, AALME-treated mice showed a dose-dependent reduction in lung damage and inflammatory cell infiltration (Fig. 7C). Western blot analysis of snout and lung tissues showed AALME treatment inhibits the levels of IAV HA and NP proteins in a dose-dependent manner (Fig. 7D and E). Concurrently, AALME reduced the mRNA expression of proinflammatory cytokines (*IL-6, IL-1β,* and *TNF-α*) and chemokines (*Cxcl10*) in the lung on day three post-infection (Fig. 7F). These results indicate that AALME plays a crucial role in protecting mice from IAV infection and mitigating IAV pathogenicity.

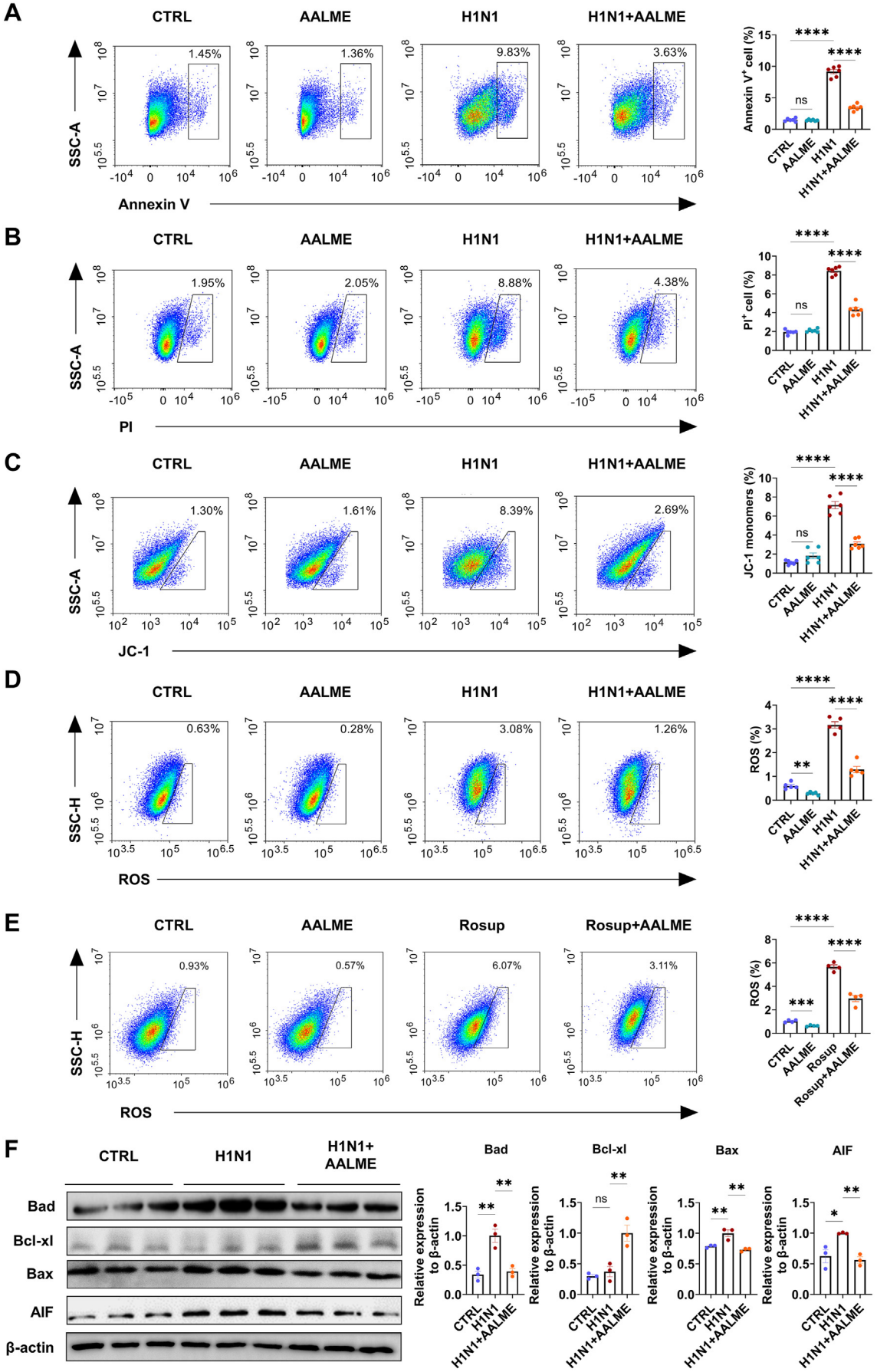

(caption on next page)

Fig. 6. AALME inhibits the IAV-induced mitochondrial apoptosis. **A–D** H1N1 virus PR8 (MOI = 0.05) and AALME (25 μg/mL) were mixed and incubated for 2 h at 4 °C before being given to A549 cells. After being incubated at 37 °C for 2 h, the mixture was removed and replaced with AALME (25 μg/mL), and they were cultured for 18 h at 37 °C. **E** A549 cells were pretreated with or without AALME (25 μg/mL) at 37 °C for 2 h, and then cells were cultured with AALME (25 μg/mL), Rosup (50 μg/mL), or AALME (25 μg/mL) + Rosup (50 μg/mL) for 12 h at 37 °C. A549 cells were subjected to Annexin V **(A)**, PI **(B)**, JC-1 **(C)**, and DCFH-DA **(D–E)** staining followed by flow cytometry. **F** Immunoblot analysis of Bad, Bcl-xl, Bax, and AIF proteins. Data are shown as the mean ± SEM. $^{*}P < 0.05$, $^{**}P < 0.01$, $^{**}P < 0.001$, $^{****}P < 0.0001$ by unpaired two-tailed Student's *t*-test. ns, no significant difference.

DISCUSSION

A. annua extract is commonly utilized in traditional Chinese medicine to treat a broad spectrum of diseases (Feng et al., 2020). Recent studies have revealed that *A. annua* extract possesses antiviral activity against herpes simplex viruses 1 and 2 (HSV-1 and HSV-2), hepatitis A virus, hepatitis B virus, bovine viral diarrhea virus, and SARS-CoV-2 infections (Seo et al., 2017; Feng et al., 2020; Nie et al., 2021). However, the antiviral studies of *A. annua* extract in the context of influenza virus (IAV) infection are less documented. In this work, we revealed hitherto unreported ways in which AALME showed strong anti-IAV effects by targeting IAV NP proteins for restricting nuclear accumulation of NP and repressing IAV-induced ROS-AIF-dependent mitochondrial apoptosis (Fig. 8). By employing this strategy, AALME directly and effectively inhibits IAV replication without relying on innate antiviral immunity, thereby limiting upper and lower respiratory tract viral infections and alleviating IAV-induced pathological lung damage. The antiviral properties of AALME suggest its potential role as a potential drug for the treatment of influenza virus infections.

Antiviral drugs can function by either attacking the virus or by eliciting a host immune response against the virus (Tompa et al., 2021). Virus-induced interferon responses, particularly type I interferon (namely, IFN-α/β) and type III interferon (namely, IFN-λ), are well understood to play an important role in host innate antiviral immunity (Ye et al., 2019). IFN-α/β and IFN-λ exert antiviral effects by inducing the expression of hundreds of interferon-stimulated genes (ISGs) via downstream JAK-STAT signaling (Ye et al., 2019). Interestingly, we observed no significant effect of AALME on the mRNA levels of IFN-α/β (*Ifn-α1* and *Ifn-β1*), IFN-λ (*Ifn-λ1* and *Ifn-λ2/3*), and ISGs (*Mx1* and *Oas2*) in the presence or absence of IAV infection *in vitro* and *in vivo*. Rather, we revealed unequivocally that AALME directly interacts with the IAV NP protein and limits its nuclear localization to restrict IAV replication. While NP is the most frequently expressed and conserved protein with multiple functions in the early and later stages of IAV infection, it is also a valid target for the development of small-molecule therapies (Krammer et al., 2018). Since the IAV protein or genome is the target of multiple clinically licensed medications, as the virus mutates, anti-IAV resistance to these drugs has appeared rapidly (Guan and Chen, 2005; Imai et al., 2020). These findings suggest that AALME may be able to target NP to block NP nuclear import, which will limit IAV infection and possibly even different influenza strains.

Host-programmed cell death is thought to be a defensive mechanism during IAV infection to inhibit viral replication, but IAV has also evolved strategies that modulate apoptosis to facilitate viral survival and establish an infection (Atkin-Smith et al., 2018). Mitochondrial-dependent pathways are critical in initiating and regulating IAV-induced apoptosis (Atkin-Smith et al., 2018). For further investigations of the molecular mechanism involved in apoptosis influenced by AALME under IAV infection, Annexin V and PI staining were employed for detecting apoptotic cells, and fluorescent mitochondrial membrane potential (MMP) probes were evaluated for mitochondrial apoptosis. Our results from flow cytometric analysis demonstrated that AALME blocked the IAV-induced early and late apoptotic processes involving mitochondrial-dependent apoptosis pathways. A high level of ROS can cause mitochondrial dysfunction and activate the mitochondrial apoptotic pathway (Foo et al., 2022). As expected, IAV infection causes ROS production in A549 cells, which AALEM inhibits. The mitochondrial death pathway involves the activation of the ratio of pro-apoptotic molecules (Bax and Bad) and anti-apoptotic molecules (Bcl-xl), which are capable of inducing mitochondrion permeabilization and allowing intermembrane proteins to be released into the cytosol, including apoptosis-inducing factor (AIF), which eventually dismantles the cell (Atkin-Smith et al., 2018). The results from Western blotting also showed that IAV infection increases the levels of Bax, Bad, and AIF in A549 cells and that AALME dramatically decreases these protein levels. AALME additionally raises the level of the anti-apoptotic protein Bcl-xl in A549 cells after IAV infection. The results reported here suggest that AALME can mechanically inhibit IAV-triggered mitochondrial-dependent apoptosis by inhibiting virus-induced ROS, Bax, and Bad production and inducing Bcl-xl production, ultimately inhibiting AIF-mediated apoptosis.

Previous studies revealed that *A. annua* extract has antiviral properties *in vitro* (Seo et al., 2017; Feng et al., 2020; Nie et al., 2021), but it is unknown whether AALME has antiviral activities *in vivo*. In this study, we observed that AALME can inhibit IAV replication in the snout and lungs via the intranasal route, as well as inhibit the expression of inflammatory factors, thereby improving the pathological lung damage caused by IAV in mice. Influenza virus is primarily transmitted via the upper respiratory tract, while blocking the IAV infection in the upper respiratory tract is essential for limiting viral transmission and spreading (Klinkhammer et al., 2018; Ye et al., 2019). Intranasal administration of AALME may interfere with the onset of IAV infection, thereby aiding in the rapid suppression of viral transmission and spread to the lungs, but additional animal models must be validated. Since nasal administration shows promise in preventing and treating respiratory viral infections (Ye et al., 2019; Alu et al., 2022), the antiviral properties of AALME in the upper respiratory tract may have important potential in inhibiting respiratory virus infection and transmission.

CONCLUSIONS

In this study, we reveal that AALME exerts significant inhibitory effects on IAV infection both *in vitro* and *in vivo*. Mechanically, AALME may block IAV infection by directly binding NP protein to restrain NP nuclear import. Furthermore, AALME can effectively inhibit IAV-triggered mitochondrial-dependent apoptosis by limiting the ROS-AIF axis. These findings suggest that AALME warrants further investigation and development as an antiviral agent against the influenza virus.

MATERIALS AND METHODS

Sample preparation

Dried *A. annua* leaves were purchased on the market (Guangxi, China) and were identified by Dr. Xun Song. Leaves were minced into powder. *A. annua* powder (500 g) was steeped in 1 L of anhydrous methanol over 3 day at 25 °C. The extract was collected and filtered before being concentrated to paste on a rotary evaporator at 40 °C and stored in DMSO for further investigation.

Ultrahigh-performance liquid chromatography-tandem mass spectrometry (UPLC-MS/MS) analysis

All chromatographic separations were performed using a Vanquish Flex UPLC system (Thermo Fisher Scientific, Bremen, Germany). For the reversed phase separation, an ACQUITY UPLC T3 column (100 mm × 2.1 mm, 1.8 μm, Waters, Milford, USA) oven was maintained at 40 °C. The

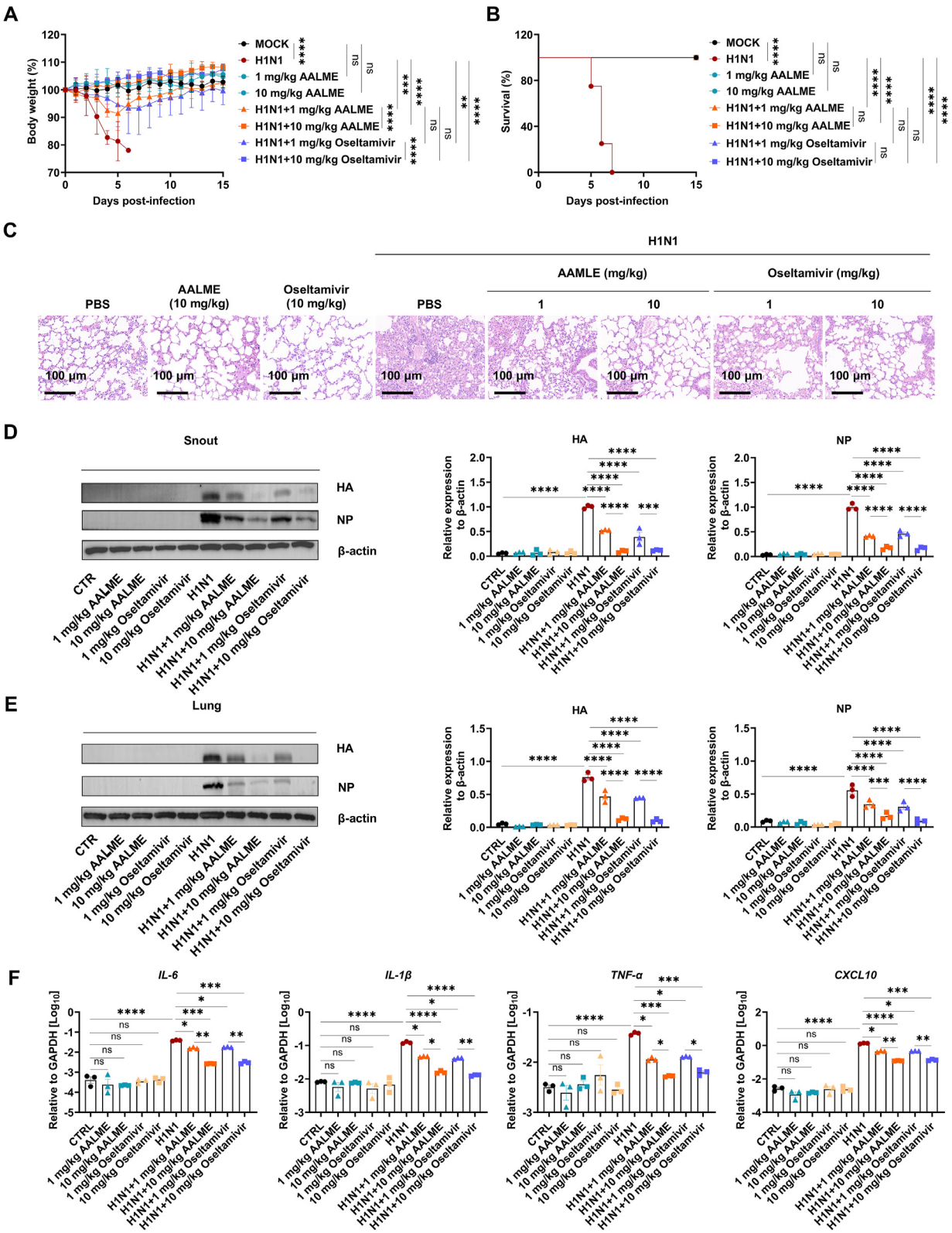

Fig. 7. Intranasal administration of AALME suppresses IAV replication in the upper and lower respiratory tracts of mice. Mice were intranasally infected with or without a lethal dose of H1N1 virus PR8, mixed or unmixed with different concentrations of AALME (1 and 10 mg/kg) or oseltamivir (1 and 10 mg/kg), and mice received AALME (1 and 10 mg/kg) or oseltamivir (1 and 10 mg/kg) by intranasal administration for three consecutive days. **A, B** Changes in body weight and survival rates of the mice were monitored over a period of 15 days after infection. **C** Histopathologic analysis of lung tissues on day 3 post-infection by H&E staining. Scale bars, 100 μm. **D, E** Immunoblot analysis of viral proteins HA and NP in the snout and lung on day 3 post-infection. Results are shown as the ratio of the specific protein to the β-actin protein and the mean ± SEM of triplicate individual experiments. **F** The mRNA levels of *IL-6*, *IL-1β*, *TNF-α*, and *Cxcl10* in the lungs on day 3 post-infection were determined by RT-qPCR. Data are shown as the mean ± SEM of four independent experiments. $^{*}P < 0.05$, $^{**}P < 0.01$, $^{***}P < 0.001$, $^{****}P < 0.0001$ by two-way ANOVA with Tukey's multiple comparison tests **(A, D–F)** or log-rank Mantel-Cox test **(B)**.

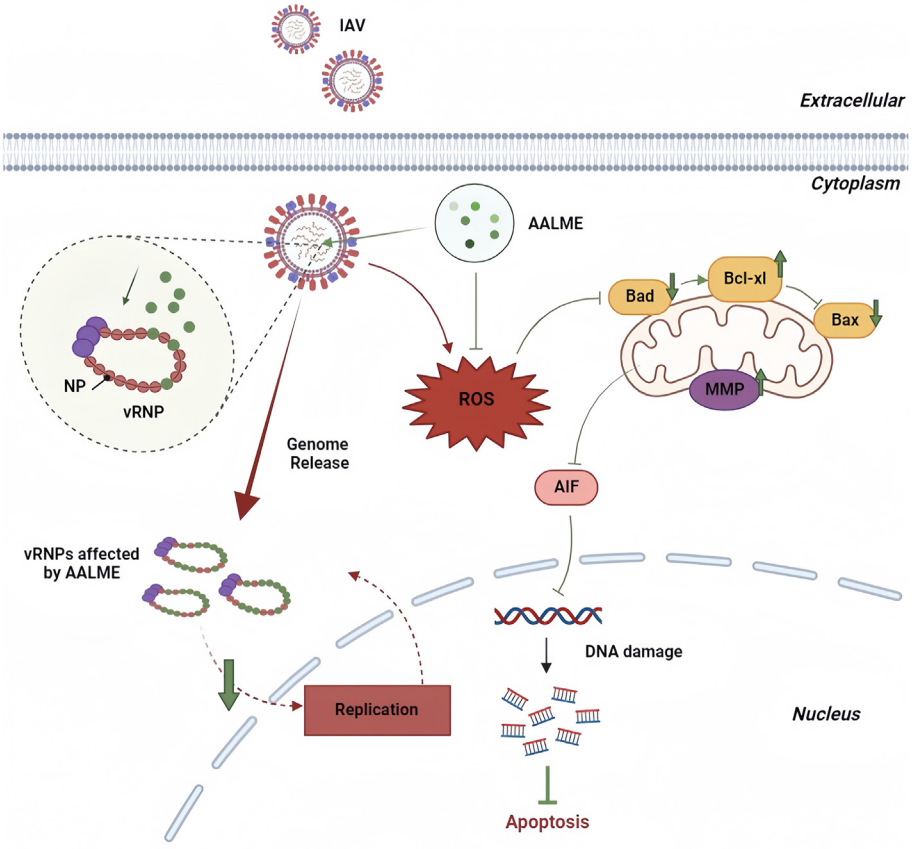

Fig. 8. *Artemisia annua* L. leaf extracts suppress influenza virus infection by targeting the viral nucleoprotein and blocking mitochondria-mediated apoptosis.

flow rate was 0.3 mL/min, and the mobile phase included solvent A (water, 5 mmol/L ammonium acetate, and 5 mmol/L acetic acid) and solvent B (acetonitrile). Gradient elution conditions were set as follows: 0∼0.5 min, 5% B; 0.5–7.0 min, 5%–100% B; 7.0–8.0 min, 100% B; 8.0–8.1 min, 100%–5% B; 8.1–11 min, 5% B.

The *Artemisia annua* L. leaf methanol extract (AALME) was acquired by the LC-MS system. To begin, all chromatographic separations were performed on a Vanquish Flex UPLC system (Thermo Fisher Scientific, Germany). To detect compounds in AALME eluted from the column, a high-resolution tandem mass spectrometer, Q-Exactive (Thermo Scientific), was used. Both positive and negative ion modes were used to operate in the Q-Exactive. MSDIAL software was used to extract and identify the peaks from the raw data. The secondary mass spectrometry data was compared to the standard database (Orbitrap TCM) established by the Shenzhen Academy of Metrology & Quality Inspection (SMQ), with matching error settings of 0.01 Da for the primary and 0.05 Da for the secondary, and a matching score of more than 70 as a trusted composition.

Cells, viruses, and animals

Madin-Darby canine kidney (MDCK) cells and adenocarcinomic human alveolar basal epithelial cells (A549 cells) (ATCC, USA) were cultured in DMEM containing 10% inactivated fetal bovine serum (FBS) (TransGen, P30922) and 1% penicillin/streptomycin (Gibco, 15140-122) at 37 °C and 5% CO_2.

H1N1 (A/PR/8/34) influenza viruses were propagated in MDCK cells supplemented with 0.5% bovine serum albumin (BSA), 1 μg/mL tosylphenylalanyl chloromethyl ketone (TPCK)-treated trypsin (Sigma, T1426), and 1% penicillin/streptomycin. Supernatants from the virus cultures were harvested on day 3 post-infection, and the virus stock was aliquoted and stored at −80 °C. Viral titers were calculated using plaque assays.

Six-to eight-week-old female C57BL/6 background mice were purchased from GemPharmatech Co., Ltd. Animal studies were carried out in specific pathogen-free (SPF) conditions. The animal experiments were authorized by the institutional Animal Care and Use Committee at Shenzhen University (approval no. IACUC-202300127).

Cytotoxicity test

MDCK and A549 cells were seeded on 96-well plates and grown to an 80%–90% confluent monolayer overnight at 37 °C. AALME and baloxavir marboxil diluted with fresh medium were applied to the cells in a gradient of concentrations (0, 10, 25, 50, 100, 150, 200, and 300 μg/mL for AALME and 0, 20, 50, 100, 200, 500, 1000, and 5000 ng/mL for baloxavir marboxil) and incubated for 24 h at 37 °C. After removing the culture medium, 10 μL of CCK-8 reagent (Dojindo, CK04) with 100 μL of fresh medium was added to each well for 1 h at 37 °C. Then the absorbance of the solution was measured at 450 nm by a microplate reader (Biotek, USA).

IAV treatment with AALME *in vitro*

MDCK or A549 cells were grown to 80%–90% confluency in plates at 37 °C. A/PR/8/34 (H1N1) (MOI = 0.05) and AALME at different concentrations were mixed and incubated for 2 h at 4 °C. Then the mixture was introduced to the cells and cultured for 2 h at 37 °C. The supernatant was then discarded, and the cells were cultured at 37 °C for different durations with fresh medium containing different concentrations of AALME and TPCK-treated trypsin (Sigma, T1426) (2.5 mg/mL for MDCK cells or 0.5 mg/mL for A549 cells). Subsequently, cells were collected at various time points post-infection for further experiments.

Cytopathic effect (CPE) assays

To determine the optimal concentration of AALME and baloxavir marboxil, MDCK and A549 cells were grown to 80%–90% confluency in 24-well plates at 37 °C, and then cells were treated for 48 h with various concentrations of AALME (0, 10, 25, 50, 100, and 200 μg/mL) and baloxavir marboxil (0, 200, 400, 600, 800, and 1000 ng/mL). Cytopathic effect (CPE) was examined under a microscope.

To evaluate the effect of AALME and baloxavir marboxil on IAV-induced CPE, MDCK and A549 cells were grown to 80%–90% confluency in 24-well plates at 37 °C. A/PR/8/34 (H1N1) (MOI = 0.05) and AALME at various concentrations (0, 5, 10, and 25 μg/mL) or baloxavir marboxil (0.4 μg/mL) were mixed and incubated for 2 h at 4 °C. Then the culture medium was replaced by the mixture for 2 h at 37 °C. The supernatant was then discarded, and the cells were cultured at 37 °C for 24 h with various amounts (0, 5, 10, and 25 μg/mL) of AALME or baloxavir marboxil (0.4 μg/mL). CPE was examined under a microscope.

Plaque assay

Monolayer MDCK cells in 12-well plates were incubated with serial dilutions of viral supernatants containing 0.05% BSA and 2.5 mg/mL TPCK-treated trypsin (Sigma, T1426) for 2 h at 37 °C. Cell monolayers were overlaid with 1.5 mL of semisolid medium containing 0.75% CMCNa, 0.3% BSA, and 2.5 mg/mL TPCK-treated trypsin and incubated at 37 °C for 40 h. Plaques were visualized after removing the semisolid medium by staining the monolayer cell with 0.2% (w/v) crystal violet solution (Sigma, C0775).

Real-time quantitative PCR (RT-qPCR)

Total RNA was extracted from cells or tissues by Trizol reagent (Takara, 9109) according to the manufacturer's protocol. cDNA synthesis using the RevertAid First Strand cDNA Synthesis Kit (Thermo Fisher, K1622). After reverse transcription, qPCR amplification was performed on the CFX96 Real-Time PCR System (Bio-Rad, USA) using Tip Green qPCR SuperMix (Transgen, China, AQ141-01). The primer sequences for gene amplification are listed in Supplementary Table S1.

Western blot analysis

Cells or tissues were lysed with RIPA buffer (Solarbio, R0010) for protein extraction and then quantified using the BCA assay kit (Beyotime, P0012), as directed by the manufacturer. The samples were then loaded with the loading buffer (FDbio, FD002) and boiled at 95 °C for 5 min. The protein samples were loaded onto a 10% sodium dodecyl sulfate-polyacrylamide gel electrophoresis (Beyotime, P0012AC) and transferred onto a polyvinylidene fluoride (PVDF) membrane (Merck Millipore, IPVH15150) for 105 min at 200 mA. After blocking with 5% skimmed milk (BioFroxx, 1172GR500) in a Tris-buffered solution containing 0.05% Tween 20 (TBST) at RT for 2 h, incubate specific primary antibodies with the membrane that loaded protein overnight at 4 °C. As primary antibodies, HA (Thermofisher, PA5-34929), NP (Thermofisher, MA5-35899), Bax (Cell signaling technology, 2772), Bcl-xl (proteintech, 26967-1-AP), Bad (proteintech, 10435-1-AP), AIF (Abcam, ab32516), Tubulin (Beyotime, AT819-1), Lamin B1 (PROTEINTECH, 66095-1-Ig), and β-actin (Abcam, ab8226) were used. Then incubated with secondary antibodies (Abcam, ab6721/ab6728) for 2 h at RT after washing by TBST. Blots were visualized by the ECL reagent kit (Meilunbio, MAO186-1) using the ChemiScope Western blot imaging system (Clinx, China), and the densitometric results were analyzed with Image J.

Cellular thermal shift assay (CETSA)

MDCK cells were infected with A/PR/8/34 (H1N1) (MOI = 0.05) for 24 h at 37 °C. Cells were then lysed with RIPA buffer (Solarbio, R0010), and the lysis solution was sonicated for 5 min under ice bath conditions before centrifugation at 4 °C, 12000 g for 15 min. After discarding the cellular debris, and 25 μg/mL of AALME or DMSO to the supernatant. The mixture was then incubated at 25 °C for 30 min prior to the CETSA heat pulse. The solutions were then heated to the indicated temperatures (45, 53, 61, and 70 °C) for 3 min before being cooled to 4 °C. After centrifugation for 20 min at 12000 g and 4 °C, the soluble supernatant was loaded with the loading buffer (FDbio, FD002) and heated at 95 °C for 5 min, subject to the Western blot assay.

Biolayer interferometry

The affinity of AALME and the His-tagged protein of IAV was determined as previously described (Liu et al. 2022). Briefly, the IAV protein was loaded in a running buffer containing PBS, 0.02% Tween-20, and 0.1% BSA. The His-tagged proteins are as follows: HA protein (Sino Biologicol, 40673-V08H), NP protein (Sino Biologicol, 11675-V08B), NA protein (Sino Biologicol, 40197-V07H), and NS1 protein (Sino Biologicol, 40011-V07E). In the running buffer, AALME was diluted to 50, 65, 75, and 100 μg/mL in PBS. Prior to use, the Ni-NTA biosensor (Forte Bio, 18–0029) tips were hydrated in the buffer for 10 min. Then, for 30 s, sensor baselines were equilibrated in the running buffer. Following that, the protein was loaded for 4 min until saturated, and the sensor was washed before immersing it in the AALME-containing well for 4 min, followed by another 4 min in running buffer. The curve fitting was performed using a 1:1 binding model and analyzed with ForteBio.

Immunofluorescence and confocal microscopy

A/PR/8/34 (H1N1) (MOI = 0.05) and AALME of 25 μg/mL were mixed and incubated at 4 °C for 2 h before being applied to monolayer MDCK cells for 1, 2, or 4 h at 37 °C. Then cells were fixed in a 4% paraformaldehyde solution (Beyotime, P0099) for 15 min before being blocked with a 3% BSA (Solarbio, A8020) solution, including 0.3% Triton X-100 (Sigma, X100), for 1 h. After blocking, cells were incubated at 4 °C overnight with an anti-NP antibody (Thermofisher, MA5-35899) solution containing 0.3% Triton X-100. Then cells were incubated for 2 h at RT with an Alexa Fluor 488-tagged anti-mouse IgG antibody (Abcam, ab150113) solution containing 0.3% Triton X-100. After staining the cells with 1 μg/mL DAPI (Cell Signaling Technology, 4083) for 20 min, they were observed under a confocal microscope and analyzed using ZEISS ZEN digital microscope software.

Flow cytometry

Monolayer A549 cells in 24-well plates were infected for 2 h at 37 °C with the mixture of A/PR/8/34 (H1N1) (MOI = 0.05) and AALME of 25 μg/mL that had previously been incubated for 2 h at 4 °C. The medium was then replaced with 25 μg/mL of AALME and cultured for 20 h at 37 °C. Cells were collected, and apoptosis was determined by flow cytometry using the following kits: Annexin V-FITC Apoptosis Detection Kit (Beyotime, C1062S), mitochondrial membrane potential assay kit with JC-1 (C2006), and Reactive Oxygen Species (ROS) Assay Kit (S0033S). For Rosup stimulation, monolayer A549 cells in 24-well plates were treated with or without AALME (25 μg/mL) at 37 °C for 2 h, and then cells were cultured with AALME (25 μg/mL), Rosup (50 μg/mL), or AALME (25 μg/mL) + Rosup (50 μg/mL) for 12 h at 37 °C. Cells were subsequently collected and determined by flow cytometry using the reactive oxygen species (ROS) assay kit (S0033S). An NovoCyte Advanteon Flow Cytometer (Agilent, China) and NOVOExpress software were used for the analysis.

The anti-IAV activity of AALME *in vivo*

Mice were intranasally infected with or without a lethal dose of A/PR/8/34 (H1N1) viruses (10^4 PFU) in the presence or absence of AALME (1 or

10 mg/kg) or oseltamivir (1 or 10 mg/kg) in a total volume of 10 μL and then received AALME (1 or 10 mg/kg) of 10 μL for three consecutive days by intranasal administration, while uninfected mice received only AALME, oseltamivir, or physiological saline. Mice were sacrificed on day 3 after infection. Snout and lung samples were collected for RT-qPCR and Western blot. Lungs were fixed in 4% paraformaldehyde and embedded in paraffin for histological sectioning and hematoxylin and eosin (H&E) staining.

Histopathological investigations

Lungs were excised and fixed for 48 h in a 4% paraformaldehyde solution (Beyotime, P0099). Samples were washed twice in 10% formalin before being dehydrated in an ethanol series (70% ethanol for 1.5 h, 80% ethanol for 30 min, 95% ethanol for 15 min and twice, and 100% ethanol for 10 min and twice). For histopathological examination, sections were stained with hematoxylin and eosin (H&E).

Statistical analysis

Results were presented as the mean ± SEM or mean ± SD and evaluated using GraphPad Prism 9.0. Statistical significance was assessed using unpaired two-tailed Student's *t*-test or one-way ANOVA with Dunnett's multiple comparisons test, two-way ANOVA with Tukey's multiple comparison tests, and the log-rank Mantel-Cox test. $P < 0.05$ was considered significant.

DATA AVAILABILITY

All the data generated during the current study are included in the manuscript. The source data and data files are available from the authors upon request.

ETHICS STATEMENT

The animal experiments were authorized by the institutional Animal Care and Use Committee at Shenzhen University (approval no. IACUC-202300127).

AUTHOR CONTRIBUTIONS

Xiwen Zhao: Writing-Original Draft, Data curation, Formal analysis, Investigation. Xuan Dai and Fuyi Wang: Validation, Investigation. Formal analysis. Chenyang Li and Xun Song: Resources, Validation. Yingying Han and Chaowei Zhang: Methodology, Validation. Zhendan He, Lu Wang, and Rongping Zhang: Founding acquisition, Supervision, Project administration. Liang Ye: Conceptualization, supervision, Funding acquisition, Writing-reviewing and Editing, Project administration.

CONFLICT OF INTEREST

The authors declare no conflicts of interest.

ACKNOWLEDGMENTS

This study was supported by grants from the National Natural Science Foundation of China (32170937), Shenzhen Medical Research Fund (SMRF, A2303015), Pearl River Talent Project of Guangdong Province (2021QN02Y426), and Shenzhen Peacock Plan Project (827/000655) to Liang Ye, and the Yunnan Provincial Key Areas Science and Technology Plan Project (202303AC100025) and Yunnan Scholar of Yunling (YNWR-YLXZ-2019-019) to Rongping Zhang.

APPENDIX A. SUPPLEMENTARY DATA

Supplementary data to this article can be found online at https://doi.org/10.1016/j.virs.2025.03.001.

REFERENCES

Abookleesh, F.L., Al-Anzi, B.S., Ullah, A., 2022. Potential antiviral action of alkaloids. Molecules 27, 903.
Alu, A., Chen, L., Lei, H., Wei, Y.Q., Tian, X.H., Wei, X.W., 2022. Intranasal COVID-19 vaccines: from bench to bed. EBioMedicine 76, 103841.
Atkin-Smith, G.K., Duan, M.B., Chen, W.S., Poon, I.K.H., 2018. The induction and consequences of Influenza A virus-induced cell death. Cell Death Dis. 9, 1002.
Badshah, S.L., Faisal, S., Muhammad, A., Poulson, B.G., Emwas, A.H., Jaremko, M., 2021. Antiviral activities of flavonoids. Biomed. Pharmacother. 140, 111596.
Chen, J., Chen, J., Wang, X., Liu, C., 2014. Anti-tumour effects of polysaccharides isolated from Artemisia annua L by inducing cell apoptosis and immunomodulatory anti-hepatoma effects of polysaccharides. Afr. J. Tradit., Complementary Altern. Med.: AJTCAM 11, 15–22.
Clarke, P., Tyler, K.L., 2009. Apoptosis in animal models of virus-induced disease. Nat. Rev. Microbiol. 7, 144–155.
de Oliveira, T.C., Silva, D.A.O., Rostkowska, C., Béla, S.R., Ferro, E.A.V., Magalhães, P.M., Mineo, J.R., 2009. Toxoplasma gondii: effects of Artemisia annua L. on susceptibility to infection in experimental models *in vitro* and *in vivo*. Exp. Parasitol. 122, 233–241.
Efferth, T., 2018. Beyond malaria: the inhibition of viruses by artemisinin-type compounds. Biotechnol. Adv. 36, 1730–1737.
Feng, X.C., Cao, S.J., Qiu, F., Zhang, B.L., 2020. Traditional application and modern pharmacological research of Artemisia annua L. Pharmacol. Therapeut. 216, 107650.
Ferreira, J., Peaden, P., Keiser, J., 2011. *In vitro* trematocidal effects of crude alcoholic extracts of Artemisia annua, A. absinthium, Asimina triloba, and Fumaria officinalis: trematocidal plant alcoholic extracts. Parasitol. Res. 109, 1585–1592.
Foo, J., Bellot, G., Pervaiz, S., Alonso, S., 2022. Mitochondria-mediated oxidative stress during viral infection. Trends Microbiol. 30, 679–692.
Guan, Y., Chen, H.L., 2005. Resistance to anti-influenza agents. Lancet 366, 1139–1140.
Imai, M., Yamashita, M., Sakai-Tagawa, Y., Iwatsuki-Horimoto, K., Kiso, M., Murakami, J., Yasuhara, A., Takada, K., Ito, M., Nakajima, N., Takahashi, K., Lopes, T.J.S., Dutta, J., Khan, Z., Kriti, D., van Bakel, H., Tokita, A., Hagiwara, H., Izumida, N., Kuroki, H., Nishino, T., Wada, N., Koga, M., Adachi, E., Jubishi, D., Hasegawa, H., Kawaoka, Y., 2020. Influenza A variants with reduced susceptibility to baloxavir isolated from Japanese patients are fit and transmit through respiratory droplets. Nat. Microbiol. 5, 27–33.
Islamuddin, M., Chouhan, G., Farooque, A., Dwarakanath, B., Sahal, D., Afrin, F., 2015. Th1-biased immunomodulation and therapeutic potential of Artemisia annua in murine visceral leishmaniasis. PLoS Neglected Trop. Dis. 9, e3321.
Juteau, F., Masotti, V., Bessière, J.M., Dherbomez, M., Viano, J., 2002. Antibacterial and antioxidant activities of Artemisia annua essential oil. Fitoterapia 73, 532–535.
Karamoddini, M.K., Emami, S.A., Ghannad, M.S., Sani, E.A., Sahebkar, A., 2011. Antiviral activities of aerial subsets of species against Herpes Simplex virus type 1 (HSV1). Asian Biomed. 5, 63–68.
Kim, E., Kim, G., Kim, B., Lim, E., Kim, S., Kim, Y., 2017. Apoptosis-induced effects of extract from Artemisia annua Linné by modulating PTEN/p53/PDK1/Akt/signal pathways through PTEN/p53-independent manner in HCT116 colon cancer cells. BMC Compl. Alternative Med. 17, 236.
Klinkhammer, J., Schnepf, D., Ye, L., Schwaderlapp, M., Gad, H.H., Hartmann, R., Garcin, D., Mahlakoiv, T., Staeheli, P., 2018. IFN-λ prevents influenza virus spread from the upper airways to the lungs and limits virus transmission. Elife 7, 33354.
Krammer, F., Smith, G.J.D., Fouchier, R.A.M., Peiris, M., Kedzierska, K., Doherty, P.C., Palese, P., Shaw, M.L., Treanor, J., Webster, R.G., García-Sastre, A., 2018. Influenza. Nat. Rev. Dis. Primers 4, 3.
Liu, Y., Song, X., Li, C., Hu, H., Li, W., Wang, L., Hu, J., Liao, C., Liang, H., He, Z., 2022. Chrysin ameliorates influenza virus infection in the upper airways by repressing virus-induced cell cycle arrest and mitochondria-dependent apoptosis. Front. Immunol. 13, 872958.
Marinas, I., Oprea, E., Chifiriuc, M., Badea, I., Buleandra, M., Lazar, V., 2015. Chemical composition and antipathogenic activity of Artemisia annua essential oil from Romania. Chem. Biodivers. 12, 1554–1564.
Medina, R.A., García-Sastre, A., 2011. Influenza A viruses: new research developments. Nat. Rev. Microbiol. 9, 590–603.
Nie, C.X., Trimpert, J., Moon, S., Haag, R., Gilmore, K., Kaufer, B.B., Seeberger, P.H., 2021. *In vitro* efficacy of Artemisia extracts against SARS-CoV-2. Virol. J. 18, 182.
Ou, L., Qin, K., Yang, Z.X., Bie, M.J., 2020. The effects and mechanisms of dihydroartemisinin on influenza A virus H1N1 induces TNF-alpha and IL-6 expression in bronchial epithelial cells. Sichuan Da Xue Xue Bao Yi Xue Ban 51, 171–177.
Özçelik, B., Kartal, M., Orhan, I., 2011. Cytotoxicity, antiviral and antimicrobial activities of alkaloids, flavonoids, and phenolic acids. Pharm. Biol. 49, 396–402.
Seo, D.J., Lee, M., Jeon, S.B., Park, H., Jeong, S., Lee, B.H., Choi, C., 2017. Antiviral activity of herbal extracts against the hepatitis A virus. Food Control 72, 9–13.
Shojaii, A., Ghods, R., 2021. The effects of Artemisia plant and its components against respiratory viruses like influenza and their mechanisms of action. Jundishapur J. Nat. Pharm. Prod. 16, e113060.
Song, D.W., Liu, G.L., Xue, M.Y., Qiu, T.X., Wang, H., Shan, L.P., Liu, L., Chen, J., 2021. *In vitro* and *in vivo* evaluation of antiviral activity of a phenylpropanoid derivative against spring viraemia of carp virus. Virus Res. 291, 198221.
Tompa, D.R., Immanuel, A., Srikanth, S., Kadhirvel, S., 2021. Trends and strategies to combat viral infections: a review on FDA approved antiviral drugs. Int. J. Biol. Macromol. 172, 524–541.
Wojtkowiak-Giera, A., Derda, M., Kosik-Bogacka, D., Kolasa-Wolosiuk, A., Wandurska-Nowak, E., Jagodzinski, P.P., Hadas, E., 2019. The modulatory effect of Artemisia

annua L. on toll-like receptor expression in Acanthamoeba infected mouse lungs. Exp. Parasitol. 199, 24–29.
Yang, X., Long, F., Jia, W., Zhang, M., Su, G., Liao, M., Zeng, Z., Chen, W., Chen, J., 2023. Artesunate inhibits PDE4 leading to intracellular cAMP accumulation, reduced ERK/MAPK signaling, and blockade of influenza A virus vRNP nuclear export. Antivir. Res. 215, 105635.
Ye, L., Schnepf, D., Staeheli, P., 2019. Interferon-λ orchestrates innate and adaptive mucosal immune responses. Nat. Rev. Immunol. 19, 614–625.